Research Article | Vol. 7, No. 9 | 1 Sep 2016 | BIOMEDICAL OPTICS EXPRESS 3403

Biomedical Optics EXPRESS

Dual-modality endomicroscopy with co-registered fluorescence and phase contrast

C. Ba,* M. Palmiere, J. Ritt, and J. Mertz

Biomedical Engineering Department, Boston University, 44 Cummington Mall, Boston, MA 02215, USA
*bacong@bu.edu

Abstract: We describe a dual-modality laser scanning endomicroscope that provides simultaneous fluorescence contrast based on confocal laser endomicroscopy (CLE) and phase-gradient contrast based on scanning oblique back-scattering microscopy (sOBM). The probe consists of a 2.6mm-diameter micro-objective attached to a 30,000-core flexible fiber bundle. The dual contrasts are inherently co-registered, providing complementary information on labeled and unlabeled sample structure. Proof of principle demonstrations are presented with ex-vivo mouse colon tissue.

OCIS codes: (170.2150) Endoscopic imaging; (180.5810) Scanning microscopy; (120.5050) Phase measurement; (170.1790) Confocal microscopy.

References and links

1. T. J. Muldoon, M. C. Pierce, D. L. Nida, M. D. Williams, A. Gillenwater and R. Richards-Kortum, "Subcellular-resolution molecular imaging within living tissue by fiber microendoscopy," Opt. Express **15**, 16413–16423 (2007).
2. M. C. Pierce, D. J. Javier and R. Richards-Kortum, "Optical contrast agents and imaging systems for detection and diagnosis of cancer," Int. J. Cancer **123**, 1979–1990 (2008).
3. W. Zhong, J. P. Celli, I. Rizvi, Z. Mai, B. Q. Spring, S. H. Yun, and T. Hasan, "In vivo high-resolution fluorescence microendoscopy for ovarian cancer detection and treatment monitoring," Br. J. Cancer **101**, 2015–2022 (2009).
4. A. F. Gmitro and D. Aziz, "Confocal microscopy through a fiber-optic imaging bundle," Opt. Lett. **18**, 565–567 (1993).
5. P. S. P. Thong, M. Olivo, K. W. Kho, W. Zheng, K. Mancer, M. Harris and K. C. Soo, "Laser confocal endomicroscopy as a novel technique for fluorescence diagnostic imaging of the oral cavity," J. Biomed. Opt. **12**, 014007 (2007).
6. M. A. A. Neil, R. Juškaitis and T. Wilson, "Method of obtaining optical sectioning by using structured light in a conventional microscope," Opt. Lett. **22**, 1905–1907 (1997).
7. N. Bozinovic, C. Ventalon, T. Ford and J. Mertz, "Fluorescence endomicroscopy with structured illumination," Opt. Express **16**, 8016–8025 (2008).
8. S. Santos, K. K. Chu, D. Lim, N. Bozinovic, T. N. Ford, C. Hourtoule, A. C. Bartoo, S. K. Singh and J. Mertz, "Optically sectioned fluorescence endomicroscopy with hybrid-illumination imaging through a flexible fiber bundle," J. Biomed. Opt. **14**, 030502 (2009).
9. K. Murari, Y. Zhang, S. Li, Y. Chen, M. J. Li and X. Li, "Compensation-free, all-fiber-optic, two-photon endomicroscopy at 1.55 μm," Opt. Lett. **36**, 1299–1301 (2011).
10. D. M. Huland, C. M. Brown, S. S. Howard, D. G. Ouzounov, I. Pavlova, K. Wang, D. R. Rivera, W. W. Webb and C. Xu. "In vivo imaging of unstained tissues using long gradient index lens multiphoton endoscopic systems," Biomed. Opt. Express **3**, 1077–1085 (2012).
11. G. Ducourthial, P. Leclerc, T. Mansuryan, M. Fabert, J. Brevier, R. Habert, F. Braud, R. Batrin, C. Vever-Bizet, G. Bourg-Heckly, L. Thiberville, A. Druilhe, A. Kudlinski and F. Louradour, "Development of a real-time flexible multiphoton microendoscope for label-free imaging in a live animal," Sci. Rep. **5**, 18303 (2015).
12. B. Viellerobe, A. Osdoit, C. Cavé, F. Lacombe, S. Loiseau, and B. Abrat, "Mauna Kea technologies' F400 prototype: a new tool for in vivo microscopic imaging during endoscopy," in Biomedical Optics 2006, 60820C-60820C. International Society for Optics and Photonics, 2006.
13. P. L. Hsiung, J. Hardy, S. Friedland, R. Soetikno, C. B. Du, A. P. Wu, P. Sahbaie, J. M. Crawford, A. W. Lowe, C. H. Contag and T. D. Wang, "Detection of colonic dysplasia in vivo using a targeted heptapeptide and confocal microendoscopy," Nat. Med. **14**, 454–458 (2008).
14. H. Li, Y. Li, L. Cui, B. Wang, W. Cui, M. Li and Y. Cheng, "Monitoring pancreatic carcinogenesis by the molecular imaging of cathepsin E in vivo using confocal laser endomicroscopy," PloS One **9**, e106566 (2014).
15. K. C. Lee, S. Sharma, J. B. Tuttle and W. D. Steers, "Origin and characterization of retrograde labeled neurons supplying the rat urethra using fiberoptic confocal fluorescent microscopy in vivo and immunohistochemistry," J. Urology **184**, 1550–1554 (2010).

#267581 http://dx.doi.org/10.1364/BOE.7.003403
Journal © 2016 Received 7 Jun 2016; revised 8 Aug 2016; accepted 8 Aug 2016; published 10 Aug 2016

Biomedical Optics EXPRESS

16. Q. T. Nguyen and R. Y. Tsien, “Fluorescence-guided surgery with live molecular navigation - a new cutting edge," Nat. Rev. Cancer **13**, 653–662 (2013).
17. W. A. Welge, a. T. DeMarco, J. M. Watson, P. S. Rice, J. K. Barton and M. A. Kupinski, “Diagnostic potential of multimodal imaging of ovarian tissue using optical coherence tomography and second-harmonic generation microscopy," J. Med. Imaging **1**, 025501 (2014).
18. C. Joo, K. H. Kim and J. F. de Boer, “Spectral-domain optical coherence phase and multiphoton microscopy," Opt. Lett. **32**, 623–625 (2007).
19. C. Liang, M. Descour, K. B. Sung and R. Richards-Kortum, “Fiber confocal reflectance microscope (FCRM) for in-vivo imaging," Opt. Express **9**, 821–830 (2001).
20. D. C. Adler, Y. Chen, R. Huber, J. Schmitt, J. Connolly and G. J. Fujimoto, “Three-dimensional endomicroscopy using optical coherence tomography," Nat. Photon. **1**, 709–716 (2007).
21. J. Xi, Y. Chen, Y. Zhang, K. Murari, M. J. Li and X. Li, “Integrated multimodal endomicroscopy platform for simultaneous en face optical coherence and two-photon fluorescence imaging," Opt. Lett. **37**, 362–364 (2012).
22. V. Tuchin, *Tissue Optics: Light Scattering Methods and Instruments for Medical Diagnosis*, Vol. 13, (Bellingham: SPIE press, 2007).
23. G. Nomarski, “Differential microinterferometer with polarized waves," J. Phys. Radium **16**, 9S-11S (1955).
24. F. Zernike, “Phase contrast, a new method for the microscopic observation of transparent objects," Physica **9**, 686–698 (1942).
25. R. Yi, K. K. Chu and J. Mertz, “Graded-field microscopy with white light," Opt. Express **14**, 5191–5200 (2006).
26. S. B. Mehta and C. J. R. Sheppard, “Quantitative phase-gradient imaging at high resolution with asymmetric illumination-based differential phase contrast," Opt. Lett. **34**, 1924–1926 (2009).
27. X. Ou, R. Horstmeyer, C. Yang and G. Zheng, “Quantitative phase imaging via Fourier ptychographic microscopy," Opt. Lett. **38**, 4845–4848 (2013).
28. A. B. Parthasarathy, K. K. Chu, T. N. Ford and J. Mertz, “Quantitative phase imaging using a partitioned detection aperture," Opt. Lett. **37**, 4062–4064 (2012).
29. C. Mann, L. Yu, C. M. Lo and M. Kim, “High-resolution quantitative phase-contrast microscopy by digital holography," Opt. Express **13**, 8693–8698 (2005).
30. C. G. Rylander, D. P. Davé, T. Akkin, T. E. Milner, K. R. Diller and A. J. Welch, “Quantitative phase-contrast imaging of cells with phase-sensitive optical coherence microscopy," Opt. Lett. **29**, 1509–1511 (2004).
31. T. N. Ford and J. Mertz, “Video-rate imaging of microcirculation with single-exposure oblique back-illumination microscopy," J. Biomed. Opt. **18**, 066007 (2013).
32. T. N. Ford, K. K. Chu and J. Mertz, “Phase-gradient microscopy in thick tissue with oblique back-illumination," Nat. Methods **9**, 1195–1197 (2012).
33. L. P. Hariri, A. R. Tumlinson, D. G. Besselsen, U. Utzinger, E. W. Gerner and J. K. Barton, “Endoscopic optical coherence tomography and laserâĂŘinduced fluorescence spectroscopy in a murine colon cancer model," Lasers Surg Med **38**, 305–313 (2006).
34. J. Mertz, A. Gasecka, A. Daradich, I. Davison, and D. Coté, “Phase-gradient contrast in thick tissue with a scanning microscope," Biomed. Opt. Express **5**, 407–416 (2014).
35. D. K. Hamilton, and C. J. R. Sheppard, “Differential phase contrast in scanning optical microscopy," J. Microscopy **133**, 27–39 (1984).
36. Y. Kawata, R. Juškaitis, T. Tanaka, T. Wilson, and S. Kawata, “Differential phase-contrast microscope with a split detector for the readout system of a multilayered optical memory," Appl. Opt. **35**, 2466–2470 (1996).
37. W. B. Amos, S. Reichelt, D. M. Cattermole and J. Laufer, “Re-evaluation of differential phase contrast (DPC) in a scanning laser microscope using a split detector as an alternative to differential interference contrast (DIC) optics," J. Microsc. **210**, 166–175 (2003).
38. T. Y. Chui, T. J. Gast and S. A. Burns, “Imaging of Vascular Wall Fine Structure in the Human Retina Using Adaptive Optics Scanning Laser Ophthalmoscopy Vascular Wall Imaging Using AOSLO," Invest. Ophthalmol. Vis. Sci. **54**, 7115–7124 (2013).
39. D. Scoles, Y. N. Sulai, C. S. Langlo, G. A. Fishman, C. A. Curcio, J. Carroll and A. Dubra, “In Vivo Imaging of Human Cone Photoreceptor Inner SegmentsIn Vivo Imaging of Photoreceptor Inner Segments," Invest. Ophthalmol. Vis. Sci. **55**, 4244–4251 (2014).
40. D. Cunefare, R. F. Cooper, B. Higgins, D. F. Katz, A. Dubra, J. Carroll and S. Farsiu, “Automatic detection of cone photoreceptors in split detector adaptive optics scanning light ophthalmoscope images," Biomed. Opt. Express **7**, 2036–2050 (2012).
41. T. N. Ford, D. Lim and J. Mertz, “Fast optically sectioned fluorescence HiLo endomicroscopy," J. Biomed. Opt. **17**, 0211051 (2012).

1. Introduction

Fluorescence endomicroscopy has garnered attention in recent years for its ability to provide histology-like high resolution images in situ and in real time. Standard non-scanning fluorescence endomicroscopy [1] is already widely used in clinical applications, especially for can-

Biomedical Optics EXPRESS

cer detection [2, 3]. Approaches that provide optical sectioning such as confocal laser endomicroscopy (CLE) [4, 5], structured illumination [6–8] or two-photon excitation [9–11] have also gained traction. For example, commercial implementations of CLE [12] have been adopted for applications ranging from disease development to drug delivery to neuroscience [13–15]. Some limitations of fluorescence imaging, however, are that it generally requires labeling with an exogenous contrast agent, few of which are approved for clinical applications [16]. Another limitation is that fluorescence reveals only what is labeled. While such specificity provides distinct advantages in many applications, it also presents disadvantages. Often, it is desirable to place the fluorescence in the context of its unlabeled environment. For example, when imaging fluorescent cells in tissue, it is often desirable to complement this with information on the surrounding unlabeled extracellular matrix, collagen distributions, vascular morphology, etc., all of which can provide pathology signatures of their own [17]. In these cases, an endomicroscope providing simultaneous fluorescence and label-free structural imaging becomes attractive [18]. We describe here such a device, which features the advantage that fluorescence and structural imaging are derived from the same illumination source and are automatically co-registered.

Two well-known label-free endomicroscopy techniques are fiber-optic-based confocal reflection microscopy (FCRM) [19] and optical coherence tomography (OCT) [20,21]. These produce signal derived from light backscattered directly from the focal plane. That is, they intrinsically reveal only sharply varying structure in the axial direction, such as layered structure of retina or the surface of skin, and cannot reveal more slowly varying structure (i.e. structure containing spatial frequencies too low to cause light to reverse its direction). Unfortunately, biological tissue is comprised mostly of such slowly varying structure since it is mostly forward scattering [22]. In addition, FCRM and OCT both suffer from speckle noise, which can compromise the information content of the acquired images.

Another candidate for label-free structural imaging is phase-contrast imaging, which is widely used in biomedical applications because it can provide images of unlabeled and almost transparent samples. However, most phase-contrast techniques are based on trans-illumination geometries that can hardly be adopted for endomicroscopy, such as Normarski differential interference contrast (DIC) [23], Zernike phase contrast [24], oblique illumination/detection [25–28] or holographic techniques [29], to name a few. One exception is phase-contrast OCT [30], which operates in an en-face geometry, but again is limited to imaging only sharply varying structures.

To address the above limitations we introduced oblique back-illumination microscopy (OBM), which produces trans-illumination-based phase-gradient contrast in an en-face geometry, meaning it can be used with arbitrarily thick samples [31]. Specifically, we showed that OBM can be configured in an endomicroscopy configuration with a flexible fiber bundle [32], where it produces speckle-free images of slowly varying tissue structures that would be impossible to observe with reflection-based contrast. However, the distal probe optics we used in our configuration consisted of a 2.6mm micro-objective flanked by two large-core (1mm) illumination fibers held together by a clasp, resulting in a probe size greater than 6 mm. Such a probe is too large, for instance, to be threaded through the 3mm utility port of a standard gastroenterological endoscope. It also precludes many potential research applications, such as in-vivo murine colon imaging [33]. We note that large-core fibers were required here to deliver sufficient LED illumination power to the sample. Laser illumination could potentially have been delivered through much smaller core fibers, but this was found to produce unacceptable speckle noise. In brief, an alternative method to OBM is required to miniaturize our probe further.

In this paper we introduce an endomicroscope device based on a variant of OBM called scanning oblique back-scattering microscopy (sOBM) [34]. In our new design, we dispense with the flanking illumination fibers, meaning our probe diameter is reduced to 2.6mm. Moreover, we complement the sOBM contrast of our endomicroscope with simultaneous fluorescence contrast, yielding a versatile dual-modality instrument of suitable geometry for clinical applica-

Biomedical Optics EXPRESS

tions.

2. Principle of sOBM

sOBM, as its name suggests, is a scanning analogue to widefield OBM, which, according to the principle of Helmholtz reciprocity, provides rigorously identical imaging [34]. A schematic of the principle of sOBM is illustrated in Fig. 1. In its original implementation focused laser light was delivered into the sample through an objective and backscattered signal was detected via two flanking optical fibers. In our new implementation the flanking fibers are dispensed with, and the backscattered signal is detected through the objective itself, by projecting an image of the focal plane onto a quadrant detector. The purpose of the quadrant detector is to measure imbalances in the backscattered laser power relative to the focus axis, in either of the lateral x or y directions, or both. These imbalances are signatures of index-of-refraction gradients within the sample that tilt the focused laser beam one way or the other depending on the direction of the gradient. Gradients at the focal point tilt the entire laser beam, whereas gradients increasingly upstream or downstream from the focal point tilt only diminishing fractions of the laser beam. As such, sOBM dominantly reveals only in-focus gradients. Said differently, objects must be in focus to produce measurable gradients – otherwise the objects appear blurred and gradients become washed out.

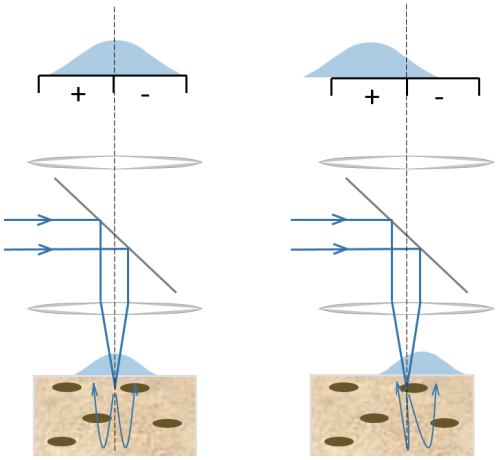

Fig. 1. Principle of sOBM based on differential split detection. In-focus phase gradients at the laser focus deflect the laser beam and lead to an asymmetric distribution of the back-scattered light with respect to the focus axis. This imbalance is detected by a differential split detector. To obtain an image, the sample must be scanned, or the laser light must be scanned and de-scanned (see setup).

sOBM is similar in concept to variants used in scanning light ophthalmoscopy, for example with an offset confocal pinhole [38] or with a split detector [39,40]. It is also akin to a technique called differential phase contrast (DPC) [35–37], with the notable difference that while the split detector is located in an object plane in sOBM, it is located in a pupil plane in DPC.

3. Setup

Our dual modality endomicroscope is detailed in Fig. 2. The laser beam (Omicron PhoxX 488nm) is directed through a polarized beam splitter and scanned by a pair of galvanometric mirrors (Cambridge Technology), and expanded by lenses L1 and L2 to fill the back aperture of the objective (Olympus UMPlanFL W 10×, NA=0.3). The beam is then focused into the

Biomedical Optics EXPRESS

proximal end of a flexible imaging fiber bundle, whereupon it is transmitted by individual fiber cores. The fiber bundle itself consists of 30,000 cores, each approximately 1.9 μm in diameter separated by an average distance of 3.3 μm (center to center). The total useful diameter of the fiber bundle is 600 μm. The distal end features a micro-objective (Mauna-Kea Technologies; 2.6 mm diameter; 14 mm length; either 1× or 2.5× magnification; 60 μm working distance; NA=0.8 water). Both the fiber bundle and the micro-objective serve to relay the laser light into the sample, producing a scanning focal spot of size roughly given by the core diameter divided by the micro-objective magnification. Two signals can be produced by this laser focus. The first is fluorescence, which is epi-collected by the micro-objective and relayed by the fiber bundle back into the microscope, whereupon it is de-scanned and relayed again into a pinhole (National Aperture, 50μm), and detected through an emission filter by a photomultiplier tube (Hamamatsu HC125-02). The net magnification from the microscope objective focal plane to the pinhole is about 28×, meaning that the image of a single fiber core at the pinhole plane is about 53μm, or slightly larger than the pinhole diameter. The fluorescence is thus obtained in the same manner as a conventional scanning confocal microscope, similar to [12].

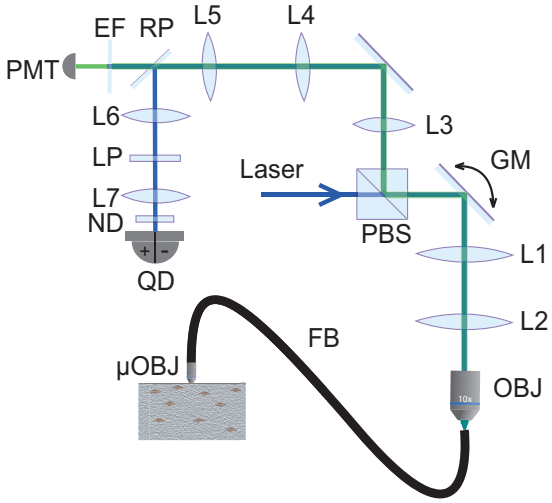

Fig. 2. Schematic of our dual modality endomicroscope. PBS, polarized beam splitter; GM, galvanometric mirrors; OBJ, microscope objective; FB, fiber bundle; μOBJ, micro-objective; RP, reflective pinhole; EF, emission filter; PMT, photomultiplier tube; LP, linear polarizer; ND, neutral density filter; QD, quadrant detector.

The second signal comes from the laser beam itself, or more precisely the portion of the beam that traverses the focal plane and is redirected toward the sample surface by multiple scattering, in a confined enough region about the focus axis that it is collected by the micro-objective. This light is de-scanned and re-imaged onto the pinhole plane in the same manner as fluorescence, but, unlike fluorescence, here we are interested in detecting only multiply backscattered light and not ballistic light (i.e. not singly backscattered light originating directly from the focal point). In fact, the pinhole is reflective. The image of the multiply backscattered light is relayed yet again onto a quadrant detector (SensL, MicroFC-60035-SMT 2×2, quadrant size: 6mm), where differences between the left/right or top/bottom quadrants yield sOBM signals corresponding to sample-induced phase gradients in the x or y directions. The net magnification from the microscope objective focal plane to the quadrant detector is 13×, meaning that the image of the proximal face of fiber bundle at the quadrant detector is about 8 mm in diameter. An additional neutral density filter (OD=0.7) is inserted before the quadrant detector to ensure

Biomedical Optics EXPRESS

this remains within its dynamic range.

Some issues to consider. In particular, spurious background light can be detected by the quadrant detector that can undermine the sOBM signal. This does not come from singly back-reflected light from the laser focus (i.e. what would normally be considered FCRM signal), because such light either goes through the pinhole or gets relayed to the 1mm gap between the SensL detector quadrants, and thus does not contribute to the sOBM image. By far, the most significant background comes instead from specular back-reflections originating from various optical interfaces in the illumination beam path. The most deleterious of these are back-reflections originating from the fiber probe, such as the interfaces at the proximal and distal ends of the fiber bundle (the former can be reduced by using an immersion objective), and interfaces within the probe micro-objective itself. To reduce these back-reflections as much as possible, we make use of two cross-polarizers (PBS and LP in Fig. 2). However this leads to only incomplete background rejection because the polarization of distal back-reflections becomes mostly scrambled through the fiber bundle. Additional rejection must be performed numerically by first acquiring a background image (no sample) and then systematically subtracting this background from subsequent sOBM images. A similar background subtraction is also performed with fluorescence images to reduce spurious autofluorescence produced by the fiber-bundle.

Finally, there is the problem of the patterned appearance of the images caused by the quasi-periodic distribution of the fiber cores. To alleviate this, we applied an iterative segmentation-interpolation algorithm that basically fills in the gaps between the fiber cores. A detailed description of this algorithm can be found in [41]. This algorithm has the advantages that it is fast (typically 2-3 iterations suffice to produce adequate results) and does not sacrifice spatial resolution or sample contrast, as opposed to, for example, Gaussian or median filtering. We note that this algorithm was initially designed for positive-only images, whereas sOBM produces both positive and negative values. We thus modified our algorithm to apply segmentation-interpolation to the positive and negative components of the sOBM images separately.

4. Results

To begin, we illustrate the benefits of our segmentation-interpolation algorithm described above. Fig. 3 shows endomicroscope images of fluorescent beads (Phosphorex 20μm) in a scattering phantom. Fig. 3(a) and (b) are simultaneously acquired fluorescence and phase-gradient images after background subtraction. The residual pattern of the fiber bundle cores is readily apparent in Fig. 3(a) (it is less apparent in Fig. 3(b) because of background subtraction). This residual pattern is largely removed in Figs. 3(c,d) by segmentation-interpolation, without significant loss in resolution or contrast. We note that the phase-gradient image reveals some unevenness of the phantom surface.

Tissue imaging experiments were performed with freshly excised mouse colon that was slit along its length and opened to expose the epithelial lumen. To ensure that the scattering medium to be imaged by sOBM was thick enough to re-direct laser illumination back toward the tissue surface by multiple scattering (i.e. thicker than the transport mean free path), the colon tissue was placed on a substrate of agarose embedded with scattering non-fluorescent polystryrene beads. To obtain fluorescence contrast, the tissue was wet with a 10^{-4} mol/L solution of acridine orange (Invitrogen) for 20 minutes prior to imaging. Imaging was performed with two different fiber probes, equipped with 1$\times$ and 2.5$\times$ micro-objectives, leading to spatial resolutions of roughly 3.3μm and 1.3μm respectively, defined by the fiber cores. The results are shown in Fig. 4, along with overlays of the two contrasts. Our frame rate was 2 frames/s, limited by the speed of our galvanometric scanners. The laser power incident on the tissue was less than 0.3 mW. Clearly apparent in the images are cell nuclei revealed by fluorescence and the brush border of the lamina propria mucosal layer revealed by sOBM. The latter provides morphological information that can potentially reveal tissue abnormalities not accessible by fluorescence. We

Biomedical Optics EXPRESS

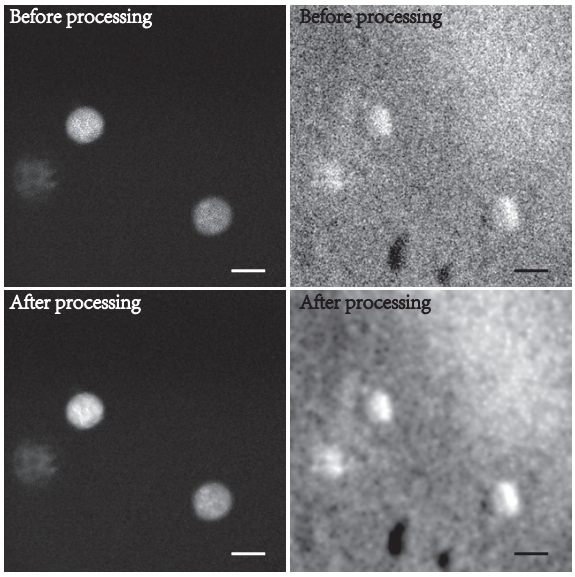

Fig. 3. Simultaneous fluorescence (left) and sOBM (right) images of 20μm beads in a scattering phantom, acquired with a 2.5× micro-objective. Top and bottom panels correspond to images before and after the application of segmentation-interpolation to remove patterning artifacts due to the fiber bundle cores (scale bar 24μm).

emphasize again that the fluorescence and phase-gradient contrasts, while representing complementary sample information, are automatically co-registered here because they arise from the same laser focus.

To evaluate the degradation of our images caused by the use of the fiber probe (i.e. the micro-objective and fiber-bundle relay), we removed this and obtained images of the same tissue through the microscope objective alone (Olympus UPlanFL N 10×, NA=0.3), as shown in Fig. 5. These have the same FoV and can be directly compared with endomicroscope images obtained through the 1× fiber probe. Despite the degradation in resolution and SNR (see discussion) caused by the fiber probe, the images appear similar and reveal the same structures.

5. Discussion

In summary, we have demonstrated, for the first time to our knowledge, a dual-modality endomicroscope that produces simultaneous, co-registered fluorescence (CLE) and phase-gradient (sOBM) contrast, with the goal of laying some groundwork for a potential future clinical device. While successful, we note that our technique is not without drawbacks.

The most egregious problem we faced came from the spurious back-reflected laser light originating from optical interfaces within our device, particularly the interfaces within the distal end of of the fiber probe. While we did our best to reject this background optically and reduce it numerically, we were only moderately successful. For example, while background subtraction is indeed effective at reducing, or even eliminating, average background, it cannot reduce the shot noise associated with this background which can compromise SNR (we note that our reference background image acquired with no sample was spatially filtered to avoid introducing even more shot noise from the background image itself). However, it should be mentioned that the fiber probes used for our demonstrations were not designed with sOBM in mind. Perhaps future designs could incorporate improved anti-reflection coatings to minimize back-reflections at the laser wavelength, or, better yet, an integrated polarizer/quarter-wave-plate isolator.

Biomedical Optics EXPRESS

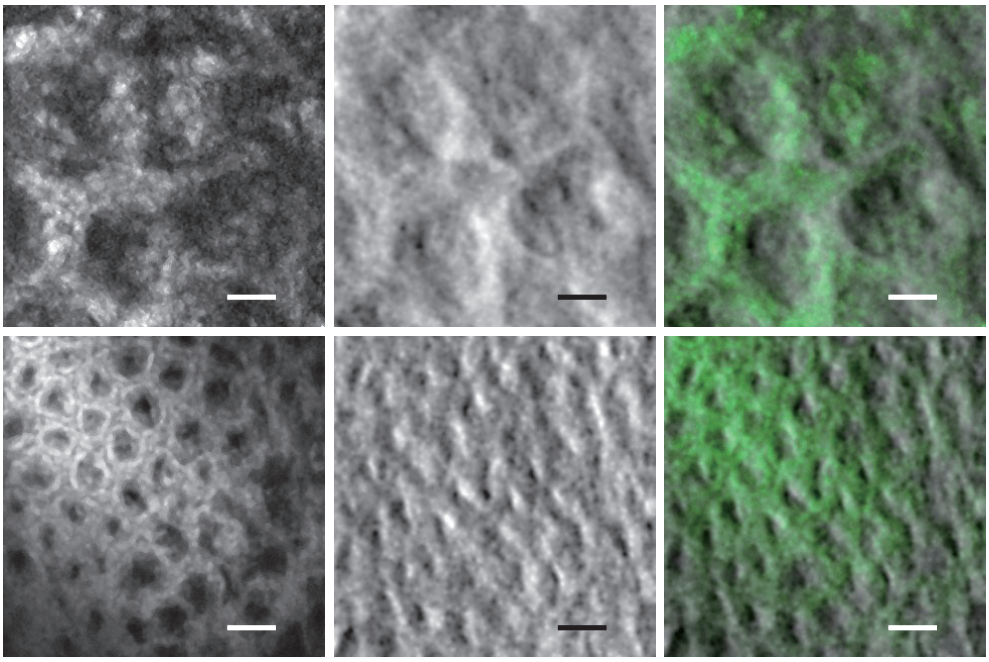

Fig. 4. Top row from left to right: fluorescence, phase-gradient and combined images of mouse colon tissue labeled with acridine orange, acquired with 2.5× micro-objective (scale bar 24μm). See also Visualization 1 for a video recorded with a frame rate of 2 fps. Bottom row from left to right, fluorescence, phase-gradient and combined images of the same sample acquired with 1× micro-objective (scale bar 60μm).

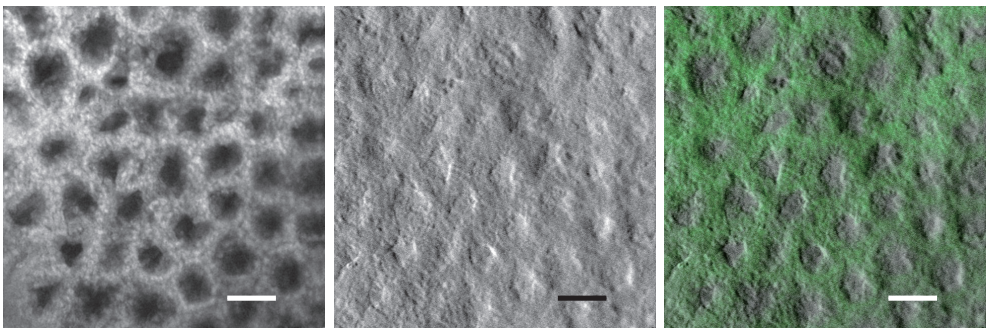

Fig. 5. From left to right: fluorescence, phase-gradient and combined images of labeled mouse colon tissue acquired directly through the microscope objective with no fiber probe (scale bar 60μm). These span the same FoV as the bottom row images in Fig. 4 and can be used to evaluate the degradation caused by the fiber probe. Also see Visualization 2 for a video recorded with this setup.

Biomedical Optics EXPRESS

Another difficulty we faced was that of limited depth penetration, which was restricted in our case by the 60μm working distance of our fiber probes. But even if this working distance had been extended, we would have been faced with the inherent limitation of sOBM that it cannot penetrate deeper than the scattering length of the laser illumination (same depth limitation as for standard DIC). For mouse colon tissue illuminated by 488nm light, we estimated this to be somewhere on the order of the probe working distance in any case. We also anticipate a few challenges when performing actual clinical imaging, such as probe stability and en-face placement, though these challenges are not new and seem to have been largely resolved in commercial instrumentation for gastro-enterological imaging [12].

Finally, we close our paper with an interesting aside. It was emphasized above that OBM and sOBM should produce rigorously identical images owing to the principle of Helmholtz reciprocity. But it was also noted that OBM, when operated with laser illumination (as opposed to LED illumination), produced unacceptable speckle noise. This speckle noise was mostly absent from our sOBM images, even though our sOBM was operated with laser illumination. Why was that? This apparent discrepancy is resolved by noting that our OBM and sOBM configurations were, in fact, not exact reciprocal analogues. Ideal laser illumination corresponds to single spatial-mode illumination. An exact reciprocal analogue sOBM would then have required single mode detection. But in our case, sOBM detection was performed with a large-area quadrant detector, meaning our detection was highly multimode. Had we replaced our large-area quadrant detector with four offset small pinholes, we would have indeed observed significant speckle noise, but as it happened this speckle noise was spatially averaged by our large-area detector so as to become effectively negligible.

Funding

This work was supported by NIH grants R01CA182939 and R21EB020851 and NSF grant CBET-1508988.